Electronic Supplementary Material (ESI) for Chemical Science.

Two Roaming Channels in the Photolysis of CH_3CHO between 328 and 308 nm.

Kin Long K. Lee,[§a] Mitchell S. Quinn,[§a] Alan T. Maccarone,[†b] Klaas Nauta,[a] Paul L. Houston,[c] Scott A. Reid, [‡b] Meredith J.T. Jordan,[b] and Scott H. Kable,*[a]

Corresponding author: Email: s.kable@unsw.edu.au

This supplementary information details the various experimental considerations that went into producing this work and a complete set of experimental data. This document consists of four sections:

(I) Experimental Setup;
(II) Preventing CH_3CHO Cluster Formation;
(III) 2D REMPI Technique.
(IV) Further Experimental data

I – Experimental Setup

All experiments were performed on a custom-built velocity-map ion imaging (VMI) spectrometer, shown in Figure S1 and described previously.[S1] The design of this spectrometer was based upon the DC-slice-imaging apparatus described by Townsend *et al*.[S2] and will not be described in detail here. Our apparatus differs in only two aspects – the distance from the interaction region to the detector is 77 cm, and the shielding electrodes are 1 mm thick. All experiments were performed using the conventional VMI (dual electrode) method, not the DC-slice method outlined in Ref. S2.

A fresh premix was prepared at the beginning of each day by freeze-pump-thawing CH_3CHO (ACS reagent, ≥99.5%, Sigma-Aldrich) primarily to minimize the presence of any water. A 5 L gas sample cylinder was filled to approximately 10 kPa with CH_3CHO and topped up with He to a total pressure of 500 kPa. A mole fraction of 1-2% CH_3CHO was used to avoid the formation of clusters (discussed further in Section II).

The CH_3CHO premix (150 – 200 kPa) was flowed through a solenoid-activated pulsed valve (General Valve Series 9), resistively-heated to 60°C. The gas is pulsed into the first of three differentially-pumped vacuum chambers, as shown in Fig S_1, where it undergoes supersonic expansion. The centre of the free jet expansion is skimmed (1 mm diameter) before entering the second chamber. The ensuing molecular beam was intersected by the counter propagated photolysis and probe lasers between the repellor (R) and extractor (L1) electrodes.

CH_3CHO photolysis was carried out over the range 30480 – 32500 cm^{-1} (328 – 308 nm) by the frequency doubled output from a Sirah Cobra Stretch dye-laser (DCM in ethanol), pumped by the second harmonic of a Quanta Ray (Beamlok) Nd:YAG laser. The light output from this laser was collimated by a pair of irises and focused in the interaction region by a 50 cm lens (0.5 – 1 mJ per pulse). The CH_3 or CO photofragments were selectively ionized using resonance-enhance multiphoton ionization (REMPI) a short time (30 – 50 ns) after photolysis.

To detect the CO fragment, a one-colour (2+1) REMPI detection scheme, resonant with the $B(^1\Sigma^+) \leftarrow X(^1\Sigma^+)$ transition, was implemented. The 230 nm ionizing light was produced by mixing the frequency-doubled light from a Quantel (TDL90) dye laser (Pyrromethene-597 dye in ethanol), with the 1064 nm fundamental from a seeded Quantel YG Nd:YAG laser. The Doppler width of the CO fragments (~2 cm^{-1}) exceeded that of our laser system. Consequently, CO images were collected by scanning the laser over the Doppler profile in 0.002 nm steps in the dye-fundamental. The power of this ionizing laser was typically ~ 0.5 mJ per pulse, tightly focused into the interaction region with an f = 50 cm lens.

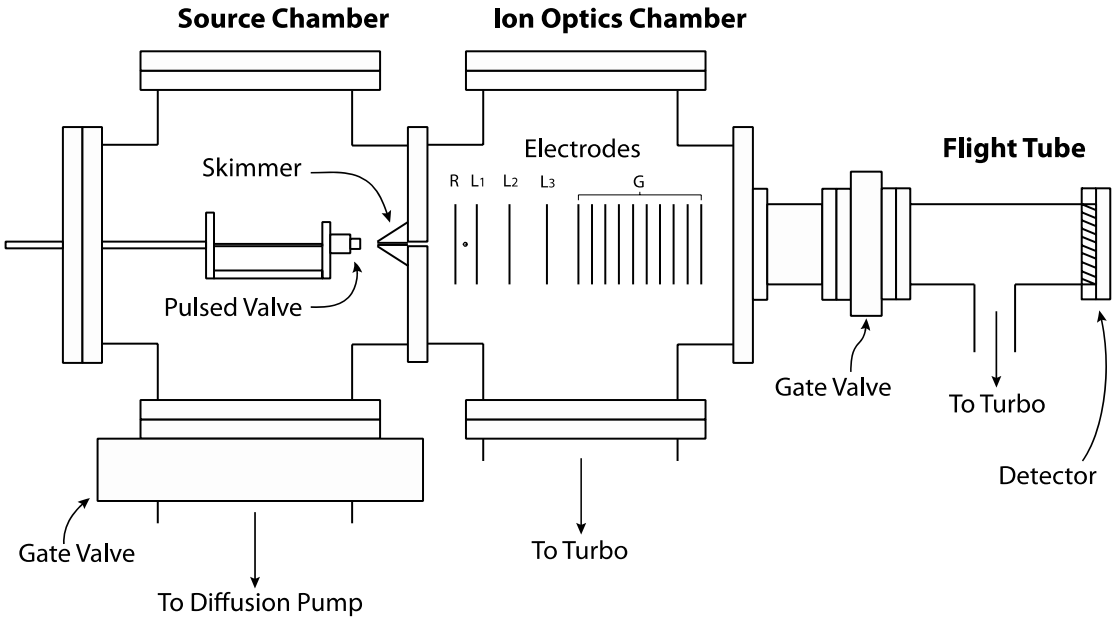

Figure S1: Schematic of experimental apparatus. The molecular beam flows left to right from the pulsed valve, through a skimmer to the interaction region between R and L1 where CH_3CHO is photolysed by one laser pulse and CO or CH_3 fragments probed by another. CO^+ or CH_3^+ ions are accelerated between the electrodes and impact the position sensitive detector at the far right.

To image of the CH_3 fragment, a separate one-colour (2 + 1) REMPI scheme is employed, resonant with the origin band of the $3p(\,^2\boldsymbol{A_2'}) \leftarrow \tilde{\boldsymbol{X}}(\,^2\boldsymbol{A_2''})$ at ~333.6 nm. The doubled output from a Lambda-Physik (LPD3001) dye laser (DCM:Pyridine-1 dye mix in methanol) was focused into the chamber by an f = 50 cm lens with the laser power typically ~1 mJ / pulse.

In all experiments, the polarization of the lasers was vertical so as to lie in the plane of the detector, thus ensuring cylindrical symmetry of the experiment. Fundamental dye laser wavelengths were measured to within 0.002 nm with a Coherent Wavemaster wavemeter.

The voltage applied to the extractor was varied slightly from day to day to ensure the VMI conditions were valid. The repeller was set to +2400 V, with the ratio of the repellor and extractor voltages being ~0.72.[S3] All other electrodes were held at ground.

Ions were accelerated towards a dual MCP detector (44 mm diameter Chevron 3040FM) coupled to a P20 phosphor screen (Wallis P47). The detector was gated so as to only detect ions with m/z 15 (CH_3) or 28 (CO) by rapidly pulsing the front of the first MCP from ground to –450 V. Note that by rapid pulsing the front of the detector there was no discernable distortion of the ion cloud.

Images and the 2D-REMPI spectra were collected with a CCD video camera (Sony XC-HR70), a NI-PCI-1410 frame-grabber board, and a custom written Labview program. Due to the position-dependent

response of the detector, all images were accumulated using an event-counting algorithm adapted from Suits and coworkers.[S4]

Background ion signal, from two sources contributed up to 15% of the signal: probe-alone signal from CH_3CHO and non-resonant pump-probe signal from vacuum pump oil. To remove this background, and to account for long-term fluctuations in probe laser power, and sample pressure, images were collected using active background subtraction. In this scheme a two-colour image is collected for 10 seconds (100 laser shots), the pump laser was then toggled off and a 10 second image of the one-colour, probe alone, image collected. This process was repeated 50 to 100 times to produce two images of 5000 to 10000 laser shots, the first being of the two-laser image, and the other the probe alone image.

Pump-alone signal from pump oil started to become significant (>5% of total signal), for pump wavelength, $\lambda > 320$ nm (when CH_3CHO signal was getting small). A further 5000-10,000 shot of the pump alone image was collected, immediately after the initial, probe substracted, two-colour, image. Active background subtraction was not required here as the signal from the pump laser was not dependent on the molecular beam, and the pump laser power was quite constant.

Each image (and background image(s)) was symmetrized along the vertical and horizontal axes, and convolved with a 2-D Gaussian (1 pixel FWHM) to smooth out any false, sharp features. The background image(s) were then subtracted from the primary, two-colour image. The CO (or CH_3) speed distribution was then obtained from the subtracted image using the BASEX program developed by Reisler and co-workers.[S5]

Our experiment was calibrated weekly using the well-known photodissociation of molecular oxygen at 225 nm.[3]

II – Preventing $(CH_3CHO)_n$ Cluster Formation

CH_3CHO clusters were found to form readily over a wide range of molecular beam conditions. Cluster formation was dependent on the source pressure, temperature, and concentration of CH_3CHO. To ensure that no clusters were being formed, we found the following conditions to be required in our apparatus: CH_3CHO mixing fraction <2% in He, backing pressure, P_0 < 200 kPa, and nozzle temperature, T_{noz} > 50°C. Passing the sample through an in-line sintered filter, containing powered $MgSO_4$ as a desiccant, greatly reduced clustering under a wide range of conditions. This suggests that H_2O is a significant factor in the formation of CH_3CHO clusters.

Due to the larger number of degrees of freedom in a cluster, it is likely that energy will be preferentially partitioned into the internal excitation of the molecule(s), leaving little for the relative translational energy of any photoproducts. In other words, photoproducts from $(CH_3CHO)_n$ dissociation will have product state distributions peaking at low kinetic and rotational energy relative to the monomer.

This purpose of this work was to investigate the origin of slow moving CO fragments, so the presence of any spurious slow moving CO from clusters, would greatly complicate the results.

Figure S2 shows the effect of clusters on the CO speed distributions. A 5% premix of CH_3CHO at a backing pressure of 200 kPa was plumbed up to the back of the nozzle heated to different temperatures, 23°C and 50°C. The sample was photolysed by 308 nm laser light, and the J_{CO} = 13 fragments selectively ionized. This particular rotational state was chosen as it clearly exhibits the two dominant product state distributions present (see main paper). The distributions have been normalized to the high-speed component. The speed distribution taken with T_{noz} = 50°C is the same as other cluster free measurements. The distribution obtained from the room temperature nozzle, however, shows an increase in the relative number of slow moving CO fragments.

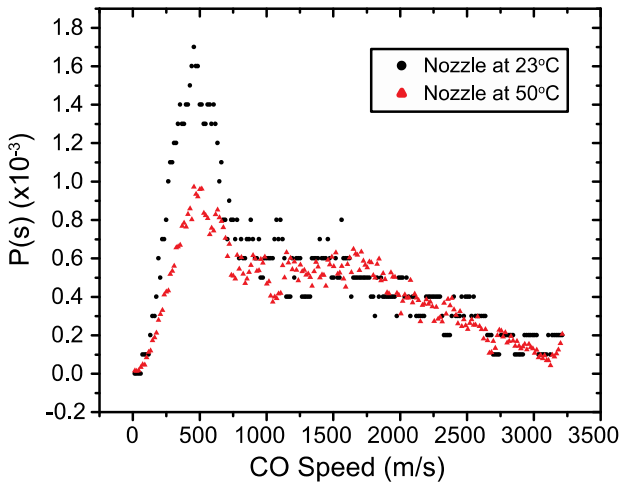

Figure S2: Speed distributions obtained from CH_3CHO dissociation at 308 nm, probing J_{CO} = 13 photofragment. Both distributions were obtained under identical conditions, from a 5% CH_3CHO in He premix, with the exception of the nozzle temperature. The distributions were chosen to clearly show the dynamical signatures of the two dominant molecular pathways, and have been normalized to the higher speed component, to show the variance in the cold component.

An unambiguous test for CH_3CHO clusters lay in the CH_3 + HCO product channel. At wavelengths shorter than 320.5 nm (373 kJ/mol) dissociation via the T_1 channel dominates. A small exit barrier present on the T_1 surface, shown in Figure 1, partitions most of the available energy into translation. Little or no energy is partitioned into the internal nodes of the fragments.[S6,S7] Consequently the dominant signal in the CH_3 fragment channel will be peaked away from zero kinetic energy, and should be readily distinct from any slow fragments.

Figure S3 shows two methyl images with, and without clusters in the molecular beam. The images were taken under similar circumstances as those shown in Figure S2, with CH_3CHO dissociated at 308 nm. Image (a) was taken under non-clustering conditions – 2% CH_3CHO in He, T_{noz} = 60°C. Image (b) however, was taken under conditions that promote clustering – 5% CH_3CHO in He, T_{noz} = 23°C. The difference between the images is stark: image (a) exhibits no discernable slow moving CH_3 fragments, distinct from Image (b), which exhibits a strong low speed CH_3 component. We used CH_3 images such as these to confirm that experiments were conducted under cluster-free conditions.

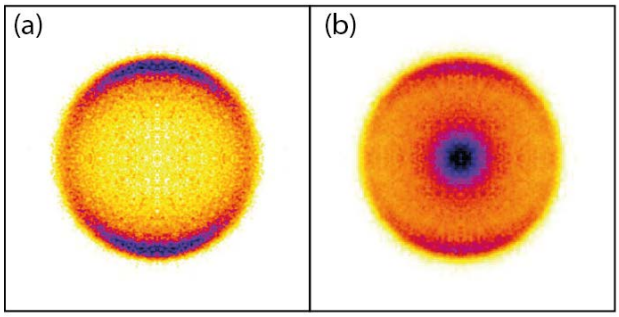

Figure S3: Velocity map images of the CH_3 fragment from photodissociation of CH_3CHO at 308 nm. The difference between the two images arises from differences in molecular beam conditions: (a) 5% CH_3CHO in He, nozzle heated to 60°C; (b) 5% CH_3CHO in He, nozzle left at room (23°C) temperature.

III – 2D Doppler-Free REMPI Ion Images

Velocity map ion imaging (VMI) has proven itself to be a highly effective experimental tool for investigating the dynamics of elementary chemical processes. Traditionally, in the investigation of photolysis reactions, as is the case for this study, an individual measurement for each rovibrational state of the photofragments is required to obtain an unambiguous picture of the reaction. This can be very time consuming. Another method, first demonstrated by Dick and co-workers in 2009,[S8] overcomes this problem by measuring the velocity of ions as a function of the ionizing laser wavelength. That is, it is possible to measure the product state distribution of a photofragment for all rovibrational states in one measurement, on a timescale equivalent to an ordinary REMPI spectrum scan. This technique records the radial and angular ion distribution as a function of laser wavelength. In this study the CO distributions were isotropic, and so the angular information was not required.

To better resolve the bandhead region in the one-colour (2+1) REMPI regime for CO detection, higher spectroscopic resolution was desired in the form of the sub-Doppler REMPI technique developed by Suits and coworkers.[9] This technique again uses a VMI apparatus, but only measures ions with zero velocity component along the direction of laser propagation, thus observing a Doppler-free REMPI spectrum.

Here, we have hybridised these two techniques, producing a Doppler-free REMPI - ion image. The speed distribution of CO fragments orthogonal to the laser propagation axis was measured as a function of the REMPI laser wavelength. Thus obtaining a Doppler-free, speed correlated REMPI spectrum. A mask with a vertical slit was placed over the detector, centered on the point where the CO velocity was zero (with respect to the laser propagation). The slit width, when combined with the non-zero recoil from the ionization step,[S9] gave the setup a spectral linewidth on the order of 0.05 cm^{-1}. A PMT was used to collect the total ion signal and a CCD camera collect the distribution of ions. The CCD collects an image, recording only the region of interest (the slit) via software mask and locating ions using the centroiding routine mentioned previously.[S4]

For each laser step, 100 images were integrated to form the speed distribution for that wavelength. The image collection software sends a trigger to step the laser and the process is repeated.

For ion expansions whose radius (r) exceeded half the slit width (W), a portion of the total ion signal will be masked, and so undercounted. To correct for this, the ion count for expansions with $r > W/2$, is multiplied by r (the pixel distance from the centre). This correction is equivalent to the function used by Suits and coworkers in Ref. S9.

As shown in Fig 2, data can be extracted in two ways from this 2D REMPI spectrum - rotational distributions as a function of speed and speed distributions as a function of rotation. It is important to reiterate that the speed distributions are still from the 'pancaked' three dimensional ion sphere projected onto the two dimensional detector. In other words the pixel intensity (ion counts) at any point is a superposition of the contributions of particles with kinetic energies equal to, and less than the maximum kinetic energy release. Consequently, when extracting out the REMPI spectra as a function of speed, the low speed REMPI will be contaminated by the higher speed component's REMPI spectrum.

To isolate the low-speed, H roaming, REMPI spectrum from the 2D spectrum two spectra are required: the first is the CO REMPI spectrum obtained by integrating over all CO speeds (i.e. integrating the whole REMPI spectrum); the second is by integrating only over CO speeds greater than 1500 ms^{-1} as mentioned above. Here the total (all-speeds) REMPI spectrum was treated as a linear combination of the high and low speed REMPI spectra. At low J(CO) (<20) the low speed component is non-zero, however, at higher J(CO) (>20) only the high-speed component contributes to the total signal (i.e. the coefficient to the low speed component is zero). Consequently, for J>20, the high speed REMPI spectrum is identical to the all-speeds REMPI. By scaling the high-speed REMPI spectrum to match the all-speeds REMPI spectrum above J=20, the difference between the spectra gives the low speed REMPI spectrum (Spectrum (B), Fig. 2)

The transition line strength does not vary significantly over this vibrational band, so an integration of the low speed and scaled high speed REMPI yields the total branching fraction over all rotational states (v = 0) without assumption.

Speed distributions are extracted from the 2D REMPI by integrating over some, or all, CO rotational state(s). This allows, theoretically, for the speed distribution of each rotational state to be extracted from the one measurement. In practice, however, there is generally insufficient ion counts for reasonable signal to noise. This is overcome by integrating over several J, as the speed distribution changes slowly with respect to the rotational state. Integrating over all J gives an overall speed distribution for this CO vibrational band (v=0).

IV – Further Experimental Data

CO ion images were measured at six photolysis wavelengths, as listed in Table 1 of the main paper. Figure S4 shows the CO recoil speeds associated with the data in Table 1. Four of these are included in Fig 3 (main text); the figure below shows all six.

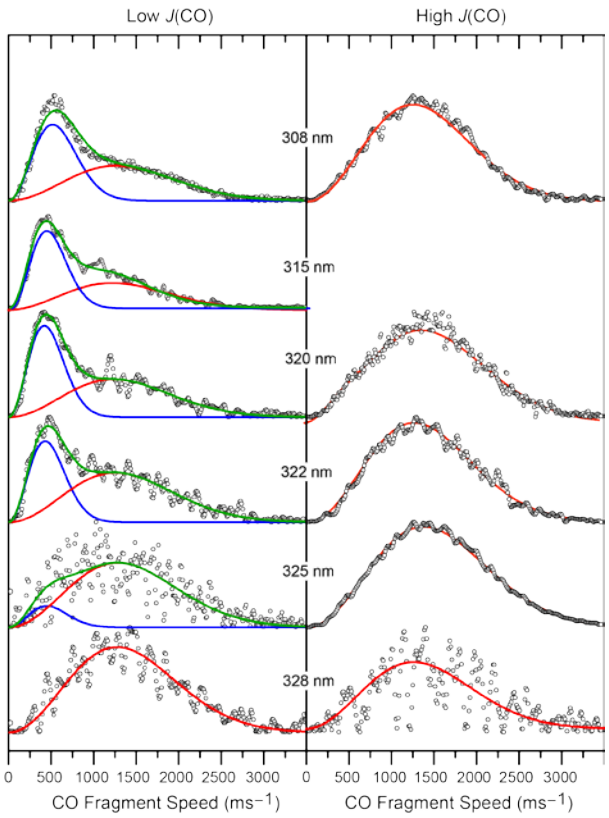

Figure S4: CO fragment recoil speed measured at different photolysis wavelengths. This is the complete set of data, corresponding to Fig 3 in the main text.

Notes and References.

* Corresponding author: Email: s.kable@unsw.edu.au

[a] School of Chemistry, University of New South Wales, Kensington, NSW, 2052, Australia

[b] School of Chemistry, University of Sydney, Sydney, NSW 2006, Australia

[c] School of Chemistry and Biochemistry, Georgia Institute of Technology, Atlanta, GA, 30332, USA.

[§] These authors contributed equally to this work and should be considered joint first authors.

[†] Present address: Department of Chemistry, University of Wollongong, NSW, 2522, Australia.

[‡] Present address: Department of Chemistry, Marquette University, Milwaukee, WI, 53201, USA.

(S1) N. Hobday, M. S. Quinn, K. Nauta, D. U. Andrews, M. J. T. Jordan, and S. H. Kable, *J. Phys. Chem. A,* 2013**,** 117, 12091

(S2) D. Townsend, M. P. Minitti and A. G. Suits, *Rev. Sci. Instrum.,* 2003**,** 74, 2531

(S3) A. Eppink and D. H. Parker, *Rev. Sci. Instrum.,* 1997, 68, 3477.

(S4) W. Li, S. D. Chambreau, S. A. Lahankar and A. G. Suits, *Rev. Sci. Instrum.,* 2005, 76, 063106

(S5) V. Dribinski, A. Ossadtchi, V. A., Mandelshtam and H. Reisler, *Rev. Sci. Instrum.,* 2002, 73, 2634

(S6) A. C. Terentis, M. Stone, and S. H. Kable, *J. Phys. Chem.*, 1994, 98, 10802

(S7) H. A. Cruse and T. P. Softley, *J. Chem. Phys.*, 2005, 122, 124303

(S8) A. Schmaunz, U. Kensy, A. Slenczka and B. Dick, *Phys. Chem. Chem. Phys*., 2009, 11, 7115

(S9) V.Goncharov, N. Herath, A. Arregui, L. Banares, A. G. Suits, *J. Phys. Chem. A* 2009, 113, 3840